



**HAL**  
open science

## **Optimizing interferences of DUV lithography on SOI substrates for the rapid fabrication of sub-wavelength features**

Olfa Karker, Romain Bange, Edwige Bano, Valerie Stambouli

► **To cite this version:**

Olfa Karker, Romain Bange, Edwige Bano, Valerie Stambouli. Optimizing interferences of DUV lithography on SOI substrates for the rapid fabrication of sub-wavelength features. *Nanotechnology*, 2021, 32 (23), pp.235301. <10.1088/1361-6528/abe3b6>. <hal-03318890>

**HAL Id: hal-03318890**

**<https://hal.univ-grenoble-alpes.fr/hal-03318890v1>**

Submitted on 25 Nov 2021

**HAL** is a multi-disciplinary open access archive for the deposit and dissemination of scientific research documents, whether they are published or not. The documents may come from teaching and research institutions in France or abroad, or from public or private research centers.

L'archive ouverte pluridisciplinaire **HAL**, est destinée au dépôt et à la diffusion de documents scientifiques de niveau recherche, publiés ou non, émanant des établissements d'enseignement et de recherche français ou étrangers, des laboratoires publics ou privés.



HAL Authorization

# 1 Optimizing Interferences of DUV Lithography on 2 SOI Substrates for the Rapid Fabrication of 3 Subwavelength Features

4 **Olfa Karker<sup>1,2</sup>, Romain Bange<sup>1,2</sup>, Edwige Bano<sup>1</sup>, Valérie Stambouli<sup>2</sup>**

5 <sup>1</sup> IMEP-LaHC, Univ. Grenoble Alpes, CNRS, Grenoble INP, 38000 Grenoble, France

6 <sup>2</sup> LMGP, Univ. Grenoble Alpes, CNRS, Grenoble INP, 38000 Grenoble, France

7  
8 E-mail: edwige.bano@grenoble-inp.fr

9  
10 Received xxxxxx

11 Accepted for publication xxxxxx

12 Published xxxxxx

## 13 **Abstract**

14 Scalable fabrication of Si nanowires with a critical dimension of about 100 nm is essential to  
15 a variety of applications. Current techniques used to reach these dimensions often involve  
16 e-beam lithography or DUV lithography combined with resolution enhancement techniques.  
17 In this study, we report the fabrication of <150nm Si nanowires from SOI substrates using  
18 DUV lithography ( $\lambda = 248$  nm) by adjusting the exposure dose. Irregular resist profiles  
19 generated by in-plane interference under masking patterns of width 800 nm were optimized to  
20 split the resulting features into twin Si nanowires. However, masking patterns of micrometre  
21 size or more on the same photomask does not generate split features. The resulting resist  
22 profiles are verified by optical lithography computer simulation based on Huygens-Fresnel  
23 diffraction theory. Photolithography simulation results validate that the key factors in the  
24 fabrication of subwavelength nanostructures are the air gap value and the photoresist  
25 thickness. This enables the parallel top-down fabrication of Si nanowires and nanoribbons in  
26 a single DUV lithography step as a rapid and inexpensive alternative to conventional e-beam  
27 techniques.

28 **Keywords:** photolithography, deep ultraviolet, silicon on insulator, nanowire

29

## 30 **1. Introduction**

31 Si nanowires (NW) are used in a variety of  
32 applications, including the recent research on field-effect  
33 transistor (FET) sensors, in particular on biosensors [1]–  
34 [4], due to their high surface-to-volume ratio and electron  
35 mobility. Alternative structures like Si nanoribbons (NR)  
36 can efficiently replace NWs in such sensing applications,  
37 where lateral critical dimension (CD) is not a crucial  
38 parameter [5]–[8]. Top-down fabricated Si NWs are  
39 generally preferred over bottom-up NWs because of their  
40 compatibility with CMOS technology. However,

41 achieving feature sizes of 100 nm and below is still  
42 challenging without industry-grade equipment, and  
43 generally requires costly e-beam lithography processes or  
44 the combination of deep-UV (DUV) lithography with size  
45 reduction methods. Methods for reducing the size of Si  
46 NWs include the use of spacers and sacrificial layers [9],  
47 mesa isolation techniques, controlled anisotropic etching  
48 [1], [10], resist trimming, or thinning down Si features  
49 through cycles of thermal oxidation and selective oxide  
50 etch. These methods extend the resolution limits of  
51 lithography and can result in feature sizes down to about  
52 10 nm, potentially. However, some of these methods are  
53 not compatible with silicon-on-insulator (SOI) substrates,

1 which are playing a growing role in advanced CMOS  
2 processes.

3  
4 Here, we present an alternative fabrication method of  
5 Si NWs from SOI substrates using DUV lithography. By  
6 taking advantage of in-plane interference and adjusting  
7 exposure parameters, it is possible to generate ridged  
8 resist features resulting in isolated twin NWs and to reach  
9 sub-wavelength CD. Interference between the incident  
10 wave and the reflected wave due to substrate reflectivity  
11 can generate vertical standing-wave roughness on resist  
12 sidewalls [11] and is generally suppressed by adding a  
13 bottom anti-reflective coating (BARC) to the resist stack  
14 [12]. In-plane interference is used in laser interference  
15 lithography (LIL) as a maskless technique to generate  
16 periodic nanodot or nanowire patterns on a large scale  
17 [13]–[15]. In this study, isolated horizontal interference  
18 patterns were observed, inducing wave variations in the  
19 resist profile, and were exploited to split Si features into  
20 twin NWs. Nanowires with a CD down to 120 nm were  
21 successfully fabricated from 800 nm mask pattern in a  
22 single step, without any thinning process, by optimizing  
23 the exposure dose. This method allows fast prototyping  
24 and scalable fabrication of NWs and NRs without the  
25 need for expensive and time-consuming e-beam  
26 lithography. Extensive optical lithography numerical  
27 simulation is conducted by ATHENA's Optolith (Silvaco)  
28 in which the experimental process flow of fabrication is  
29 respected. The simulation results confirm that the air gap  
30 value (between the mask patterns and the photoresist  
31 surface), photoresist thickness and the mask patterns  
32 width are the key factors allowing the introduction of  
33 diffractions in the conventional DUV lithography  
34 process.

## 36 2. Materials and methods

37 SOI substrates with 70-nm-thin single-crystal Si film  
38 and 145-nm-thin buried oxide were spin-coated by UV5  
39 (Microchemicals) positive photoresist (PR) at 4000 rpm  
40 for an expected thickness of about 0.525  $\mu\text{m}$ , and baked  
41 for 60 s at 130  $^{\circ}\text{C}$ . Substrates were aligned with a  
42 quartz/chrome mask holding linear patterns of widths 0.8,  
43 1.0 and 1.3  $\mu\text{m}$  using a Süss Microtech MJB4 mask  
44 aligner in vacuum contact mode. The samples were  
45 exposed for 1 s by a Hg/Xe deep-UV (DUV) source with  
46 a nominal power of 4  $\text{mW}\cdot\text{cm}^{-2}$  at wavelength 248 nm.

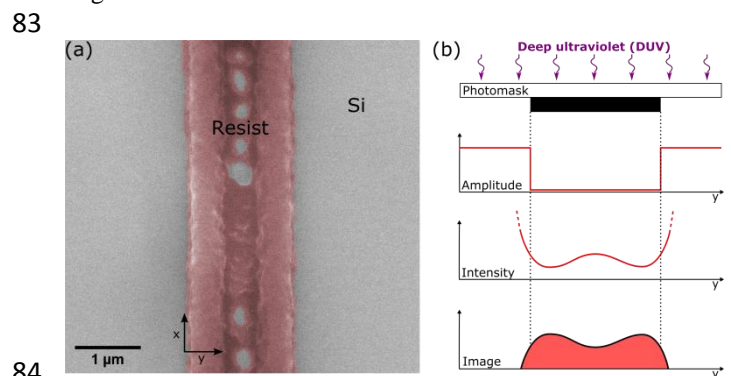
47 For optimization purposes, as will be discussed  
48 further, the exposure time ranged from 0.9 to 2.6 s. A  
49 post-exposure bake was applied for 90 s at 130  $^{\circ}\text{C}$  before  
50 the samples were bathed in AZ326MIF developer and  
51 rinsed with DIW. The topmost Si film was etched by SF<sub>6</sub>  
52 reactive ionic etching (RIE) using a Corial 200 IL RIE,

53 and etch depth was controlled by end-point detection  
54 (EPD). Resist stripping was then conducted with AR300-  
55 76 remover and the surface was cleaned by oxygen  
56 plasma.

## 57 3. Results

58 Exposure parameters for DUV lithography were  
59 initially adapted from standard Si processes to be used on  
60 SOI substrates. Conformity of the resulting PR and Si  
61 patterns to the target dimensions was controlled on bulk  
62 Si substrates using the same parameters. However, on  
63 SOI substrates, it is noticeable that resist patterns are not  
64 correctly resolved. The overall footprint of the linear  
65 patterns is wider than the expected 0.8, 1.0 and 1.3  $\mu\text{m}$ .  
66 As shown on Figure 1a and 1b, the resist features have  
67 curved lateral walls, inclined with an angle of about 75 $^{\circ}$   
68 with the surface, and a ridged cross-section split by a  
69 groove in the middle.

70  
71 The feature shown in Figure 1a was obtained using  
72 UV5 resist and exposing it for 1.3 s, which was the  
73 standard for Si. Since it is a positive resist, the middle  
74 groove indicates a partially overexposed area centred  
75 underneath opaque chrome patterns. The spatial profile of  
76 resist features provides information about the actual  
77 distribution of light intensity in the resist volume  
78 compared to the expected amplitude generated by the  
79 masking patterns, as illustrated in Figure 1b. The cross-  
80 sectional shape can also be found in the plane of the Si  
81 surface, as parabolic lobes are formed instead of right  
82 angles.

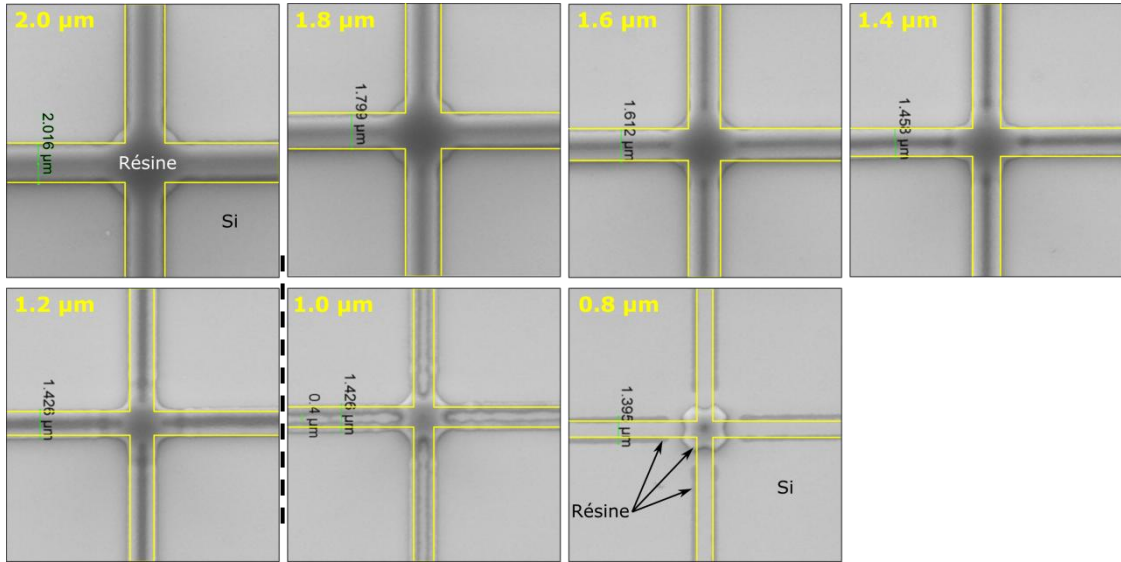


84  
85 **Figure 1.** (a) Top-view SEM images of typical resist features obtained  
86 by deep-UV lithography of a linear pattern of 1.3  $\mu\text{m}$  width on 70/145  
87 nm SOI substrates. The photoresist is colorized in red. (b) Schematic  
88 cross-section view of the light profile under a chrome pattern and the  
89 resulting positive PR feature.

90  
91 The morphology of resist features was investigated  
92 using SEM with variable target width. Figure 2 shows the  
93 resist image of crossed linear mask patterns, which range  
94 from 0.8 to 2  $\mu\text{m}$  in width. The exposure time was fixed  
95 at 2 s to deliver a dose of 8  $\text{mJ}\cdot\text{cm}^{-2}$ . SEM images show

1 that the middle groove is almost absent from 2  $\mu\text{m}$   
 2 patterns and becomes deeper and wider as the target  
 3 width decreases, until the total splitting of the features  
 4 under 1  $\mu\text{m}$ . The peak resist thickness on isolated lines  
 5 ranges from 0.5  $\mu\text{m}$  for wide lines down to about 0.1  $\mu\text{m}$

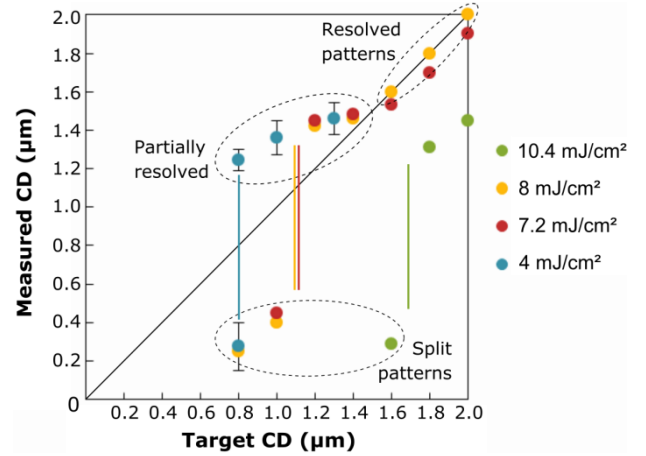
6 for split nanolignes. Regarding the measured width,  
 7 patterns of width 1.6  $\mu\text{m}$  and more appear to be  
 8 transferred with high fidelity, whereas smaller patterns  
 9 generate a footprint of limit width 1.4  $\mu\text{m}$  approximately.



**Figure 2.** Top-view SEM images of UV5 resist features formed on an SOI substrate from intersecting mask patterns, with a width ranging from 0.8 to 2.0  $\mu\text{m}$ , using DUV lithography (248 nm) at an exposure dose 8  $\text{mJ}\cdot\text{cm}^{-2}$ . Target patterns are drawn as yellow frames.

The results presented above indicate that the resist profile varies non-linearly with the Cr mask pattern width at a set exposure dose. In this case, a critical target width between 1.0 and 1.2  $\mu\text{m}$  represents the "splitting threshold" where the centre groove due to induced exposure is deep enough to reach the substrate. This threshold is illustrated as a dashed line in Figure 2.

The influence of exposure dose was also conducted to optimize process parameters. Several samples coated with PR of the same thickness were exposed for 1 to 2.6 s with a surface power density fixed at 4  $\text{mW}\cdot\text{cm}^{-2}$ . All other process parameters were identical between the samples and the resulting resist features after development was studied by SEM.



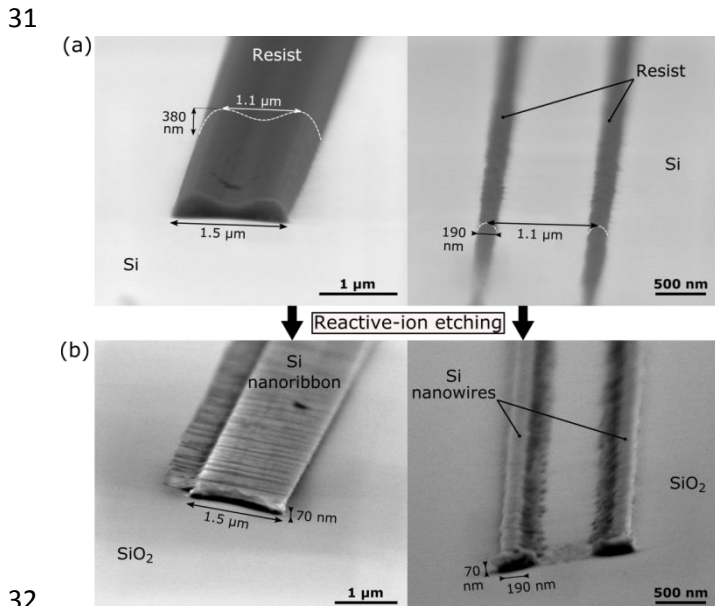
**Figure 3.** Average measured critical dimension (CD) of resist features as a function of mask target CD for different exposure doses of UV5 resist on SOI. Error bars correspond to the standard deviation, based on the measurements of about 100 nanostructures obtained with the optimal experimental dose.

Figure 3 shows the plot of the average measured critical dimension (CD) as a function of target width, for different exposure doses. A single mask pattern may result in whole resist features or split ones. In this case, the resulting CDs are displayed as two separate populations, as can be seen at  $\text{CD}_{\text{target}} = 0.8 \mu\text{m}$  for the sample exposed by 4  $\text{mJ}\cdot\text{cm}^{-2}$ .

Results show that the actual resist width varies non-linearly as a function of target width along with the mask

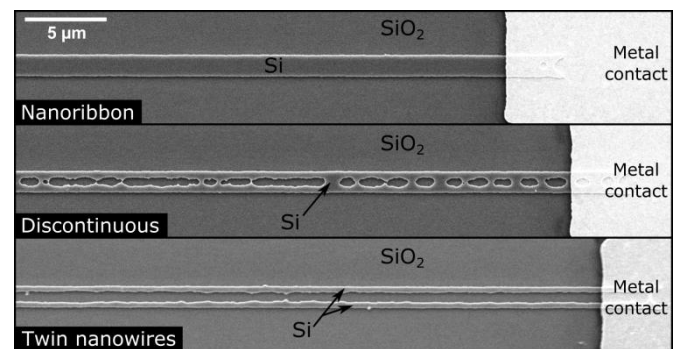
1 patterns' range. Only the largest targets ( $CD > 1.5 \mu\text{m}$ )  
 2 are resolved accurately with a moderate exposure dose of  
 3  $7\text{--}8 \text{ mJ}\cdot\text{cm}^{-2}$ . With a larger dose, a bigger volume of resist  
 4 is made soluble to the developer and thus the patterns are  
 5 reasonably narrower. Oppositely, under-exposure results  
 6 in wider resist patterns. However, under a critical target  
 7 width of about  $1.5 \mu\text{m}$ , data no longer fits with the  
 8 bisector line as the resist features displayed a wider  
 9 footprint than expected. These partially resolved features  
 10 do result as single lines of resist, but with a linewidth  
 11 print bias and a deep central groove which may produce  
 12 holes on silicon. When the target width is further  
 13 decreased, the centre groove reaches the full depth of the  
 14 resist film, thus splitting the feature completely and  
 15 lowering the CD dramatically. This splitting threshold is  
 16 correlated with exposure dose, as illustrated with vertical  
 17 lines in Figure 3, despite being difficult to measure  
 18 accurately due to the discrete nature of mask pattern  
 19 widths.

20  
 21 It appears that the splitting phenomenon of resist  
 22 patterns depends both on a target width and DUV  
 23 exposure dose. Therefore, it can be controlled and used to  
 24 form different types of Si nanostructures after etching of  
 25 the 70-nm-thin active Si film, as shown in Figure 4.  
 26 Whole patterns result in Si nanoribbons of rectangular  
 27 cross-section with an aspect ratio of about 20:1, or quasi-  
 28 planar structures. Split patterns result in two parallel  
 29 nanowires of rectangular section, each with a 2:1 to 6:1  
 30 aspect ratio.

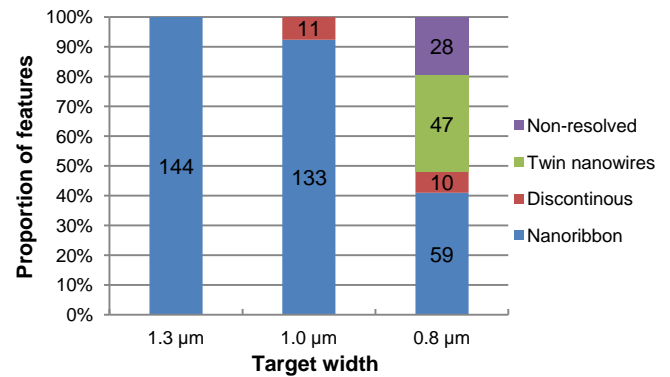


32  
 33 **Figure 4.** (a) Side-view SEM images of resist features resulting from  
 34  $1.3 \mu\text{m}$  (left) and  $0.8 \mu\text{m}$  (right) mask patterns and the same exposure  
 35 dose of  $4 \text{ mJ}\cdot\text{cm}^{-2}$ . (b) SEM images of the resulting Si features after dry  
 36 etching by  $\text{SF}_6$  RIE and before plasma cleaning.

37 However, as mentioned previously, it was observed  
 38 that a single mask pattern and exposure dose can result in  
 39 different levels of splitting. This is probably caused by  
 40 non-uniformities in the resist film thickness after spin-  
 41 coating, which might be significant due to the small size  
 42 ( $2 \times 2 \text{ cm}$ ) and square shape of the SOI samples. The  
 43 sample size for the lithography was limited to  $2 \times 2 \text{ cm}$   
 44 dies due to process constraints further in the flow. A  
 45 statistical study was conducted to evaluate the  
 46 distribution of split and whole Si patterns for three main  
 47 target widths, at a fixed exposure dose of  $4 \text{ mJ}\cdot\text{cm}^{-2}$ .  
 48 Figure 5 shows typical nano-ribbon and parallel nanowire  
 49 structures formed from identical  $0.8 \mu\text{m}$  Cr lines, as well  
 50 as an intermediary, "discontinuous" state. Thinner mask  
 51 patterns may also not be resolved at all in certain  
 52 occurrences.



53  
 54 **Figure 5.** Top-view SEM images of the different types of Si  
 55 nanostructures resulting from DUV lithography with identical  $0.8 \mu\text{m}$   
 56 wide linear patterns on a single SOI substrate, followed by reactive ion  
 57 etching. Si features are colourized in blue and coated with metal on the  
 58 right end.



59  
 60 **Figure 6.** A statistical distribution of the different types of Si  
 61 nanostructures, based on 144 features obtained on a single wafer from 3  
 62 target widths after photolithography ( $\text{UV5}$  resist with  $4 \text{ mJ}\cdot\text{cm}^{-2}$   
 63 exposure dose) and etching of the topmost layer.

64  
 65 The proportion of each type of structure obtained from  
 66 a single SOI substrate and single exposure was evaluated  
 67 qualitatively, based on 144 patterns from each of the  
 68 three Cr line widths, and the results are reported in Figure  
 69 6. It appears that 7 to 8 % of patterns with target width  
 70  $0.8$  or  $1.0 \mu\text{m}$  are partially split (discontinuous), while

1 none of the patterns with target width 1.3  $\mu\text{m}$  display any  
2 discontinuity. Among 0.8  $\mu\text{m}$  patterns, 19 % are not  
3 resolved at all which means the resist was completely  
4 washed away on that spot. The remaining 0.8  $\mu\text{m}$  patterns  
5 are composed of 41 % nanoribbons and 33 % nanowires.  
6 The observed differences for a single target width are  
7 attributable to a thinner local resist film and divergence of  
8 the near-field light beam. There should be a continuous  
9 distribution of resist thickness across these patterns,  
10 affecting the depth of the groove and thus the splitting  
11 condition. This is consistent with observations on process  
12 variations: it was observed that by increasing or  
13 decreasing the development time, the proportion of  
14 unresolved or nanoribbon patterns would increase  
15 respectively, but the proportion of intermediary states  
16 (discontinuous and twin nanowires) would remain the  
17 same. However, further accurate measurements of the  
18 resist thickness would be required to confirm this  
19 hypothesis.  
20

21 Based on all these results, it appears that an optimal  
22 exposure dose can be determined to produce Si  
23 nanoribbons and nanowires from a single SOI substrate  
24 and using a single photolithography and etching process.  
25 With our process parameters, this dose was fixed at  
26 around 4  $\text{mJ}\cdot\text{cm}^{-2}$ . It appears that the process window for  
27 obtaining twin nanowires reliably is very narrow. The  
28 conventional lithography system used for this study was  
29 limited by a fixed power density of 4  $\text{mW}\cdot\text{cm}^{-2}$ , and focus  
30 bias could not be tuned. This optimized process enables  
31 to virtually achieve a critical dimension of about 150 nm,  
32 which is lower than the working wavelength of 248 nm,  
33 without the need for expensive e-beam lithography and  
34 only using a standard chrome/quartz photomask of CD  
35 0.8  $\mu\text{m}$ . The drawback of this method is a lack of control  
36 over the splitting and lack of reproducibility regarding the  
37 morphology of resulting nanostructures, especially the  
38 irregular width of parallel nanowires.

#### 39 4. Discussion

40 In this study, process conditions were determined by  
41 adjusting mainly exposure time. This parameter affects  
42 the effective development threshold of the photoresist,  
43 whereas parameters that affect light intensity contrast –  
44 such as the initial resist thickness, top Si thickness and  
45 buried oxide thickness – were fixed. Indeed, identical  
46 samples cut from a single SOI wafer were used  
47 throughout the experiments and pre-exposure parameters  
48 for PR were mostly unchanged to ensure reproducibility  
49 of the measurements and compatibility with standard Si  
50 processes on the photolithography line. Also, the research  
51 facilities used in this study did not allow full tuning of the  
52 process window. Variations of resolution with Cr pattern

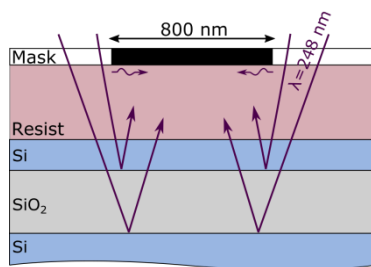
53 width were also studied and results indicate that split-  
54 patterning may happen similarly with wider Cr lines as  
55 the exposure dose increases. This method enables to  
56 fabricate split nanolines efficiently by tuning the  
57 exposure dose based on target CD.

58  
59 Experiments were conducted to identify the cause of  
60 pattern splitting and attempt to overcome it. Optical  
61 properties of SOI substrates differ drastically from bulk  
62 Si wafers due to the stacking of thin films having  
63 different refractive indexes (Figure 7). Specifically, SOI  
64 surfaces are much more reflective than Si. While  
65 substrates with high UV reflectivity increase the effective  
66 dose that is absorbed by the PR, interference of incident  
67 and reflected light also decreases light intensity over the  
68 substrate. It is possible to lower the reflectivity at the  
69 resist/substrate interface by depositing a bottom anti-  
70 reflective coating (BARC) before coating the substrates  
71 with PR. BARCs absorb light and minimize substrate  
72 reflectivity by creating destructive interference between  
73 incident and reflected light. To evaluate the effect of  
74 substrate reflectivity on the splitting of resist features, we  
75 compared the previous results with samples treated with  
76 BARC. SOI substrates were spin-coated with a DUV30  
77 BARC (Brewer Science) at 3000 rpm for 45 s to form a  
78 50 nm thin layer, which is the optimal thickness to negate  
79 the reflectivity. BARC was baked for 45 s at 180  $^{\circ}\text{C}$  to be  
80 stabilized before the PR was deposited. Positive PR was  
81 deposited, exposed and developed following the standard  
82 process described previously. Then, BARC and active Si  
83 layers were etched using  $\text{SF}_6$  RIE with an observed etch  
84 rate ratio of 14:1. Visual inspection through optical  
85 microscopy revealed similar irregular resist profiles to the  
86 ones formed without BARC. It appears that the base  
87 substrate reflectivity might not be the main cause of  
88 pattern splitting, but rather the inhomogeneous  
89 distribution of light intensity, and the interference of  
90 laterally reflected light due to the photomask being  
91 mostly clear.  
92

93 Irregular resist profiles can be caused by low  
94 uniformity of the film thickness, which is negatively  
95 affected in the case of spin-coating on small and/or non-  
96 circular substrates. On the SOI dies that were used in this  
97 study, we noticed that a resist edge bead is formed during  
98 spin-coating and is particularly abrupt in the angles. This  
99 artefact can induce an air gap between the resist film and  
100 the photomask, despite the vacuum contact mode, thus  
101 lowering the effective resolution depending on the  
102 position along the substrate's surface. To assess the  
103 influence on resist features, edge bead removal (EBD)  
104 was attempted by locally dissolving the over thickness  
105 around the edges of the SOI dies after spin-coating.

1 However, microscopy observations revealed that EBD  
 2 had no positive effect on the resolution of resist patterns.  
 3 Similarly, PR was spin-coated at a higher rotation speed  
 4 to lower the height of edge beads, with no effect on resist  
 5 profile either. Therefore, uniformity of resist thickness  
 6 does not seem to be a predominant cause of pattern  
 7 splitting.

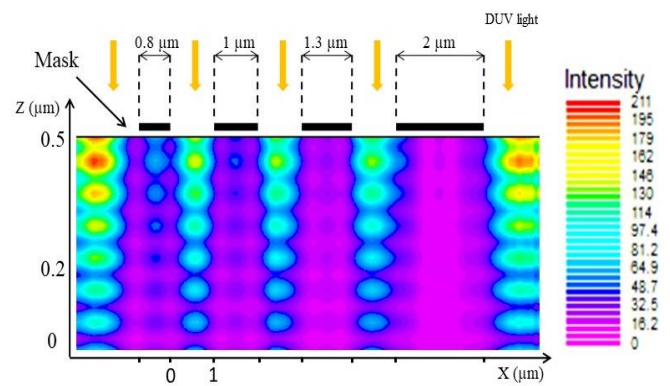
8  
 9 The most probable cause of the observed resist profile  
 10 is the diffraction of DUV light by chrome patterns under  
 11 a critical width. According to the Huygens-Fresnel  
 12 principle, obstruction of the beam by the metal edges of  
 13 chrome patterns could generate new wavefronts, and  
 14 constructive interference between the first diffraction  
 15 orders could generate the ridged image in the resist  
 16 profile. Moreover, even with perfect contact, lateral  
 17 distribution of light intensity on the resist surface is  
 18 inhomogeneous because the finite air gap thickness  
 19 creates a diffraction pattern under the mask. However, the  
 20 air gap could not be measured and further studied in these  
 21 experiments.



23  
 24 **Figure 7.** Simplified schematic cross-section view of the reflected and  
 25 diffused light supposedly contributing to constructive interference under  
 26 the mask patterns.

27  
 28 The numerical simulation offers more flexibility than  
 29 experimental work, in the study of the fabrication  
 30 parameters such as the air gap and photoresist thickness.  
 31 It also improves the understanding of the optical theory  
 32 behind the generated irregular resist profiles. Thus, an  
 33 extensive numerical two-dimensional DUV lithography  
 34 process simulation was conducted by using ATHENA's  
 35 Optolith to supplement the real experiments done in the  
 36 laboratory. Optolith tool performs all key steps of the  
 37 optical lithography processing including calculation of  
 38 the 2D aerial imaging of the mask patterns, simulation of  
 39 the light intensity propagation through photoresist and  
 40 calculation of the exposure distribution, post-exposure  
 41 bake and calculation removal of the exposed  
 42 photoresist[16]. To determine the final simulation profiles  
 43 of the photoresist, the aerial image, exposure and  
 44 development were simulated. Initially, the elementary  
 45 process parameters and conditions, counting mask data,  
 46 UV light intensity, the gap between photoresist and mask,

47 exposure time, photoresist thickness, development time,  
 48 were described as the basic operations to create the input  
 49 file of the simulation[17]. Afterwards, the aerial image  
 50 simulation is conducted to show the illumination of the  
 51 mask from the top by the incident DUV light source. All  
 52 along with the exposure simulation, the DUV light  
 53 propagation is simulated. Following, the post-exposure  
 54 bake (PEB) and the development rate distribution in the  
 55 photoresist is obtained. Afterwards, the aerial image is  
 56 transferred into the resist. Figure 8 shows the cross-  
 57 section of the 2D light intensity distribution under the  
 58 line-shaped mask patterns of different widths inside the  
 59 photoresist (named bulk image) for mask patterns of  
 60 different widths  $d=0.8 \mu\text{m}$ ,  $1 \mu\text{m}$ ,  $1.3 \mu\text{m}$ ,  $2 \mu\text{m}$   
 61 respectively.



62  
 63 **Figure 8.** Bulk image simulation showing the mask patterns and the  
 64 light intensity distribution in the photoresist below the photomask under  
 65  $d=0.8 \mu\text{m}$ ,  $1 \mu\text{m}$ ,  $1.3 \mu\text{m}$  and  $2 \mu\text{m}$ ,  $d$  is the width of the line pattern.  
 66 Distances between mask patterns are equally respected.

67 The light at the bottom of the photoresist (the exposed  
 68 photoresist, parts not covered with the mask patterns) is  
 69 gradually scattering owing to the light diffraction effect.  
 70 The middle part of the photoresist regions covered by the  
 71 chrome mask patterns show also incident light  
 72 distribution that also gradually scatter due to the light  
 73 diffraction. The amount of light diffraction at the  
 74 photoresist region under opaque mask features is directly  
 75 proportional to the width size of the mask patterns.  
 76 Following, the development of the exposed photoresist is  
 77 simulated and figure 9 shows the resulting photoresist  
 78 profiles.

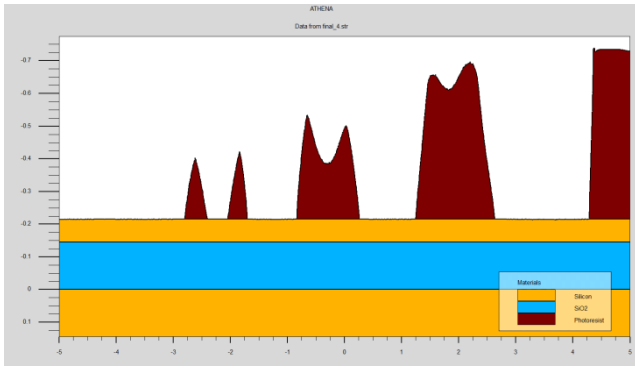


**Figure 9.** 2D simulation of the resulting photoresist profile after insolation and then development for different mask features widths  $d=0.8 \mu\text{m}$ ,  $0.1 \mu\text{m}$ ,  $1.3 \mu\text{m}$ ,  $2 \mu\text{m}$  (from left to right)

The resulting profiles show a complete splitting of the photoresist corresponding to the  $0.8 \mu\text{m}$  mask patterns and this is completely in agreement with the experimental results shown in figure 4. The photoresist profiles after development for larger mask patterns shows also an approximate shape of splitting (not completed) but with a double sine wave shape. The resulting profiles of the photoresist reflect the behaviour of the light distribution at the photoresist according to the bulk image. Thus, the light intensity when reaches a threshold value, the photoresist will get the appropriate energy to release the reaction and to turn liquid, otherwise, it will not be removed in the development step. Thus, the thickness of the photoresist is a key parameter to generate the splitting behaviour of the photoresist as the rate penetration of the light intensity should cross the total depth of the photoresist layer.

The near field or Fresnel diffraction regime can be applied in the case of operating proximity and contact exposure systems which is the case of our experimental and simulation process. So the light passing through the mask results in a diffraction pattern that directly pings on the resist surface as there is no lens between the mask and the resist on the wafer. This means that the created aerial image depends on the near field diffraction pattern. So for the moment if we consider a line-shaped mask pattern of a small width about the same size as the wavelength, and according to the Huygens's principle applied to a straight wavefront (DUV light) striking an obstacle (mask pattern), the edges of the wavefront bend after passing around the mask pattern and this process is called diffraction [18]. For small mask patterns, the amount of bending is more extreme, logical with the fact that wave characteristics are most noticeable for interactions with objects about the same size as the wavelength. This is

noticeable from the gradual intensity rises near the edges of the mask features (obstacle). Adding to that and because of the diffractions effects, the light binds away from the mask features resulting in the resist exposure at the region underneath the opaque mask patterns. Considering now that a small gap is separating the mask and the photoresist on the wafer. The diffracted waves (binding) are assumed to be incident on the mask aperture and as the gap increases the destructive and constructive interferences between the Huygens wavelets emanating around the mask feature arise resulting in the apparition of the intensity distribution within the middle part of the non-exposed region. Simulation results of the same process but at gap value of zero show no splitting behaviour of the photoresist. For a targeted and reproducible process, additional experimental work (according to the simulation results) on the air gap fluctuation and resist thickness can be conducted to increase the yield of split nanolines.

## 5. Conclusion

In this paper, we report a fabrication process of Si nanostructures with sub-wavelength critical dimension involving deep-UV wave interferences lithography. Lithographic process parameters were optimized to take advantage of irregular resist profiles obtained on SOI substrates due to in-plane interference. We show that optimal exposure dose, exact gap value, photoresist thickness and specific mask patterns size can be determined to elaborate resist features with different morphologies, resulting in Si linear structures of nanoribbon or nanowire type. Using these optimal exposure parameters, mark patterns of width  $0.8 \mu\text{m}$  can be used to generate nanowires down to  $150 \text{ nm}$  wide, along with high aspect-ratio nanoribbons, from a single SOI substrate. The method presented here enables fast and cost-effective pattern transfer at a potentially large scale, compared to e-beam lithography which has a similar resolution, at the expense of reproducibility and fine CD control. This process can be combined with the subsequent trimming to reduce the size of the Si NWs, e.g. through thermal oxidation cycles, and enables the parallel fabrication of NR FETs and twin NW FETs from SOI substrates.

## Acknowledgements

This work has been supported by Grenoble INP AGIR funds. The authors thank SOITEC for providing the SOI wafers and PTA for the training and access to clean room facilities.

## 1 References

- 2 [1] E. Stern *et al.*, "Label-free immunodetection with  
3 CMOS-compatible semiconducting nanowires.,"  
4 *Nature*, vol. 445, no. 7127, pp. 519–22, 2007,  
5 doi: 10.1038/nature05498.
- 6 [2] W. U. Wang, C. Chen, K. Lin, Y. Fang, and C.  
7 M. Lieber, "Label-free detection of small-  
8 molecule–protein interactions by using nanowire  
9 nanosensors," *Proc. Natl. Acad. Sci.*, vol. 102, no.  
10 9, pp. 3208–3212, 2005.
- 11 [3] A. Gao *et al.*, "Signal-to-Noise Ratio  
12 Enhancement of Silicon Nanowires Biosensor  
13 with Rolling Circle Amplification," *Nano Lett.*,  
14 vol. 13, pp. 4123–4130, 2013, doi:  
15 10.1021/nl401628y.
- 16 [4] T. Adam and U. Hashim, "Highly sensitive  
17 silicon nanowire biosensor with novel liquid gate  
18 control for detection of specific single-stranded  
19 DNA molecules.," *Biosens. Bioelectron.*, vol. 67,  
20 pp. 656–61, 2015, doi:  
21 10.1016/j.bios.2014.10.005.
- 22 [5] N. Elfström, A. E. Karlström, and J. Linnros,  
23 "Silicon nanoribbons for electrical detection of  
24 biomolecules," *Nano Lett.*, vol. 8, no. 3, pp. 945–  
25 949, 2008, doi: 10.1021/nl080094r.
- 26 [6] E. Stern *et al.*, "Label-free biomarker detection  
27 from whole blood," *Nat. Nanotechnol.*, vol. 5, no.  
28 2, pp. 138–142, 2009, doi:  
29 10.1038/nnano.2009.353.
- 30 [7] X. Duan, Y. Li, N. K. Rajan, D. A. Routenberg,  
31 Y. Modis, and M. A. Reed, "Quantification of the  
32 affinities and kinetics of protein interactions  
33 using silicon nanowire biosensors," *Nat.*  
34 *Nanotechnol.*, vol. 7, pp. 401–407, 2012, doi:  
35 10.1038/nnano.2012.82.
- 36 [8] K. Sun *et al.*, "Effect of subthreshold slope on the  
37 sensitivity of nanoribbon sensors,"  
38 *Nanotechnology*, vol. 27, no. 28, p. 285501,  
39 2016, doi: 10.1088/0957-4484/27/28/285501.
- 40 [9] Y. Choi, J. Zhu, J. Grunes, J. Bokor, and G. A.  
41 Somorjai, "Fabrication of Sub-10-nm Silicon  
42 Nanowire Arrays by Size Reduction  
43 Lithography," *J. Phys. Chem. B*, vol. 107, no. 15,  
44 pp. 3340–3343, 2003.
- 45 [10] A. Gao *et al.*, "Silicon-nanowire-based CMOS-  
46 compatible field-effect transistor nanosensors for  
47 ultrasensitive electrical detection of nucleic  
48 acids," *Nano Lett.*, vol. 11, no. 9, pp. 3974–3978,  
49 2011, doi: 10.1021/nl202303y.
- 50 [11] C. Wang *et al.*, "Small angle x-ray scattering  
51 measurements of lithographic patterns with  
52 sidewall roughness from vertical standing  
53 waves," *Appl. Phys. Lett.*, vol. 90, no. 193122,  
54 pp. 1–3, 2007, doi: 10.1063/1.2737399.
- 55 [12] S. K. Selvaraja, P. Jaenen, W. Bogaerts, D. Van  
56 Thourhout, P. Dumon, and R. Baets, "Fabrication  
57 of photonic wire and crystal circuits in silicon-on-  
58 insulator using 193-nm optical lithography," *J.*  
59 *Light. Technol.*, vol. 27, no. 18, pp. 4076–4083,  
60 2009, doi: 10.1109/JLT.2009.2022282.
- 61 [13] L. Prodan *et al.*, "Large-area two-dimensional  
62 silicon photonic crystals for infrared light  
63 fabricated with laser interference lithography,"  
64 *Nanotechnology*, vol. 15, no. 5, pp. 639–642,  
65 2004, doi: 10.1088/0957-4484/15/5/040.
- 66 [14] J.-H. Seo *et al.*, "Nanopatterning by Laser  
67 Interference Lithography: Applications to Optical  
68 Devices," *J. Nanosci. Nanotechnol.*, vol. 14, no.  
69 2, pp. 1521–1532, 2014, doi:  
70 10.1166/jnn.2014.9199.
- 71 [15] V. I. Bredikhin *et al.*, "Interference  
72 Nanolithography with a UV Laser," *Tech. Phys.*,  
73 vol. 49, no. 9, pp. 1191–1195, 2004, doi:  
74 10.1134/1.1800241.
- 75 [16] S. Clara, "ATHENA User 's Manual 2D  
76 PROCESS SIMULATION SOFTWARE," vol.  
77 95054, no. August, 2004.
- 78 [17] Z. F. Zhou and Q. A. Huang, "Comprehensive  
79 simulations for ultraviolet lithography process of  
80 thick SU-8 photoresist," *Micromachines*, vol. 9,  
81 no. 7, 2018, doi: 10.3390/mi9070341.
- 82 [18] A. J. Bourdillon, C. B. Boothroyd, J. R. Kong,  
83 and Y. Vladimirovsky, "A critical condition in  
84 Fresnel diffraction used for ultra-high resolution  
85 lithographic printing," *J. Phys. D. Appl. Phys.*,  
86 vol. 33, no. 17, pp. 2133–2141, 2000, doi:  
87 10.1088/0022-3727/33/17/307.